Accuracy Enhancement with Processing Error Prediction and Compensation of a CNC Flame Cutting Machine Used in Spatial Surface Operating Conditions

Shenghai Hu, Manhui Zhang*, Yunshan Cui, Rui Xue & Zhaozhen Yang

College of Mechanical and Electrical Engineering, Harbin Engineering University, Harbin, Heilongjiang Province,150001, China
*E-mail: zhangmanhui@hrbeu.edu.cn

Abstract. This study deals with the precision performance of the CNC flame-cutting machine used in spatial surface operating conditions and presents an accuracy enhancement method based on processing error modeling prediction and real-time compensation. Machining coordinate systems and transformation matrix models were established for the CNC flame processing system considering both geometric errors and thermal deformation effects. Meanwhile, prediction and compensation models were constructed related to the actual cutting situation. Focusing on the thermal deformation elements, finite element analysis was used to measure the testing data of thermal errors, the grey system theory was applied to optimize the key thermal points, and related thermal dynamics models were carried out to achieve high-precision prediction values. Comparison experiments between the proposed method and the teaching method were conducted on the processing system after performing calibration. The results showed that the proposed method is valid and the cutting quality could be improved by more than 30% relative to the teaching method. Furthermore, the proposed method can be used under any working condition by making a few adjustments to the prediction and compensation models.

Keywords: *CNC flame-cutting machine; compensation; FEA; finite element analysis; processing errors; thermal errors.*

1 Introduction

The CNC flame-cutting machine is a piece of basic manufacturing equipment in modern industrial production that is used in fields such as shipbuilding, aerospace and other industrial departments [1]. Precision performance is of great importance to the CNC flame-cutting machine, which determines the quality of the workpiece and the application range of the machine. Many studies have indicated that the main factors affecting the accuracy of the workpiece are geometric errors and thermal deformations of the machine tool; their share among the total number of processing errors is above 70% [2,3]. Consequently, in order to effectively improve processing efficiency, establishing quantitative description models of geometric errors and thermal errors, and constructing an

Received October 29th 2016, Revised February 26th, 2017, Accepted for publication March 6th, 2017.
Copyright ©2017 Published by ITB Journal Publisher, ISSN: 2337-5779, DOI: 10.5614/j.eng.technol.sci.2017.49.1.5

exact mapping relationship between them and the processing errors, and applying rational error compensation ways, are key subjects that have received extensive attention in the CNC machine tool field [4].

As for the geometric error elements of the CNC flame-cutting machine in the existing literature, kinematic calibration technology [5] has been mainly adopted to obtain accurate geometric parameters. Teaching [6-8] is considered the major compensation method in the machining operation process. However, although the teaching process currently is the main way to improve the accuracy of flame-cutting in production workshops, as it is the error compensation in a 'constant' temperature state it not only lacks thermal deformation data of the workpiece and real-time data of non-uniform temperature field, but it also includes detection errors, which means that a great improvement space still exists.

As for the temperature deformation elements, such as thermal errors and integrated errors in the CNC flame-cutting machine, although the related methods are not clearly analyzed in the existing literature, if an analytical approach to CNC machine tools [9] is used, they can still be divided into two categories: 'detection' and 'prediction'. The only difference is in the method of implementation.

Related to processing error modeling and error compensation analysis of the CNC flame-cutting machine, although comprehensive effects of the overall error elements have not been reported in the existing literature, considering that the relative motion relationship is consistent during material removal in the machining process, it is known that homogeneous transformation matrices [10,11] of the CNC machine tool can still be adopted to construct error models of the workpiece and error compensation models of the machine tool for which only the related error elements need to be set up adaptively according to the topological structure.

In this study, a self-developed CNC flame-cutting machine [12] used under spatial surface operating conditions was taken as an example. An accuracy enhancement method with processing error prediction and real-time compensation is proposed to improve the cutting quality by modifying the integrated geometric and thermal errors existing in both the machine tool and the workpiece. Moreover, FEA testing procedures and thermal dynamic modeling analysis for the thermal deformation elements were carried out respectively. Experimental studies on the actual cutting environment were conducted to verify the validity of the proposed method when compared with the generally used teaching method.

2 Processing Error Prediction and Compensation Models

To meet the digital agile cutting technique requirements of large-size fabrication holes on complex spatial curved surfaces, a CNC flame-cutting machine designed using the metamorphic principle is presented in [12]. The mechanical components and the application situation on the curved surface are shown in Figure 1, while the operation flowcharts of the variable trajectory and variable pose characteristics are also illustrated in [12].

Figure 1 Mechanical components and working conditions of the CNC flame-cutting machine.

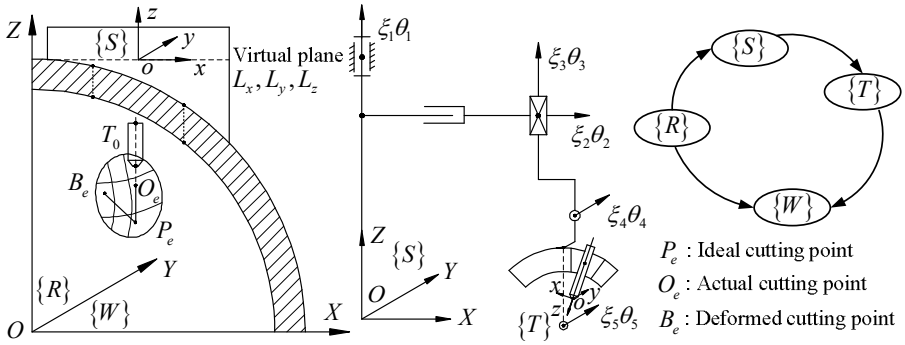

Figure 2 Machining coordinate systems of the forming process of a workpiece.

As shown in Figure 2, the required machining coordinate systems in the forming process of the workpiece are set for the CNC flame processing system shown in Figure 1. The workpiece coordinate system $\{W\}$ is set by the cylindrical profile and installed locations of a large-scale workpiece and the world coordinate system $\{R\}$ is equal to $\{W\}$. As for the machine coordinate system $\{S\}$, its axis directions are consistent with those in $\{W\}$ and its origin is determined by the virtual plane with four supporting points. As for the tool coordinate system $\{T\}$, its origin is located at the endpoint of the cutting tool and its orientations are based on the cutting tool's axis and the theoretical plane of the transmission chain.

Based on the configuration shown in Figure 2 and the setting conditions of the four machining coordinate systems, the following ideal transformation matrix can be constructed using the HTM method:

$$\begin{cases} {}^{R}\mathbf{T}_{W}^{ideal} = \mathbf{I}_{4\times 4}, \quad {}^{R}\mathbf{T}_{S}^{ideal} = Trans(L_x,\ L_y,\ L_z) \\ {}^{S}\mathbf{T}_{T}^{ideal} = \exp(\hat{\xi}_1\theta_1)\exp(\hat{\xi}_2\theta_2)\cdots\exp(\hat{\xi}_5\theta_5)\cdot\exp(\hat{\xi}_{st}{}^{i}) \end{cases} \tag{1}$$

where $Trans(\cdot)$ is the translation transformation matrix, L_x, L_y, L_z are the origin offset distances between $\{R\}$ and $\{S\}$. $\exp(\cdot)$ is the exponential product operator in screw theory [13], θ_k and ξ_k are the kinematic variables and the screw coordinates of joint $k(k=1,\cdots,5)$, $\xi_{st}{}^{i}$ is the constant screw coordinate related to the initial configuration from $\{T\}$ to $\{S\}$. These expressions can be easily obtained from the nominal parameters of the working condition and the machine tool.

The coordinate transformation relationships given in Eq. (1) are suitable for an ideal cutting situation in a CAD/CAM machining environment, while the influence of error elements in the CNC flame processing system should be taken into account with an accurate forming process for the actual cutting situation. As shown in Table 1, the overall errors of the machine tool and workpiece are classified and represented by the transformation matrix.

Table 1 Classification results of error elements in the workpiece and the CNC flame cutting machine.

Reference frame	Ideal situation	Geometric errors	Calibration situation	Thermal errors	Integrated errors	Actual situation
$\{W\}$	$P_{x,y,z}^{W}$	--	--	--	Δp_w	$Q_{x,y,z}^{W}$
$\{R\}$	${}^{R}\mathbf{T}_{W}^{ideal}$	--	${}^{R}\mathbf{T}_{W}^{e}$	--	--	${}^{R}\mathbf{T}_{W}^{real}$
$\{R\}$	${}^{R}\mathbf{T}_{S}^{ideal}$	$\Delta\mathbf{T}_{S}^{e}$	${}^{R}\mathbf{T}_{S}^{e}$	$\Delta\mathbf{T}_{S}^{thermal}$	--	${}^{R}\mathbf{T}_{S}^{real}$
$\{S\}$	${}^{S}\mathbf{T}_{T}^{ideal}$	$\Delta\mathbf{T}_{T}^{e}$	${}^{S}\mathbf{T}_{T}^{e}$	--	$\Delta\mathbf{T}_{T}^{thermal}$	${}^{S}\mathbf{T}_{T}^{real}$

In Table 1, the geometric errors $\Delta\mathbf{T}^{e}$ are the 'steady state' parameters related to the reference frame. They can be determined by calibration. The thermal and integrated errors, $\Delta\mathbf{T}^{thermal}$, are not only related to the reference position but also to the non-uniform temperature field during the flame-cutting, which means those are 'transient' parameters obtained by the effective prediction model and the on-line temperature variables. Taking the integrated function of all error elements into account, the real transformation matrix of the machining coordinate systems can be expressed as:

$$\begin{cases} {}^{R}\mathbf{T}_{W}^{real} = \mathbf{I}_{4\times4}, \quad {}^{R}\mathbf{T}_{S}^{real} = \Delta\mathbf{T}^{thermal} \cdot \Delta\mathbf{T}^{e} \cdot {}^{R}\mathbf{T}_{S}^{ideal} = \Delta\mathbf{T}_{S}^{thermal} \cdot {}^{R}\mathbf{T}_{S}^{e} \\ {}^{S}\mathbf{T}_{T}^{real} = \Delta\mathbf{T}^{thermal} \cdot \Delta\mathbf{T}^{e} \cdot {}^{S}\mathbf{T}_{T}^{ideal} = \Delta\mathbf{T}_{T}^{thermal} \cdot {}^{S}\mathbf{T}_{T}^{e} \end{cases} \tag{2}$$

where ${}^{R}\mathbf{T}_{S}^{e}, {}^{S}\mathbf{T}_{T}^{e}$ are the calibration models with geometric errors; the obtaining method is clearly derived in [14]. The analytic models of $\Delta\mathbf{T}_{S}^{thermal}, \Delta\mathbf{T}_{T}^{thermal}$ can be uniformly expressed as:

$$\Delta\mathbf{T}^{thermal} = {}^{\mathrm{U}}\mathbf{T}_{\mathrm{V}}^{thermal} \cdot \left({}^{\mathrm{U}}\mathbf{T}_{\mathrm{V}}^{e} \right)^{-1}, \quad \mathrm{U} = R,S \quad \mathrm{V} = S,T \tag{3}$$

$$\begin{cases} \Delta\mathbf{T}^{thermal} = Trans(\Delta t_x, \Delta t_y, \Delta t_z) Rot(x, \Delta t_\alpha) Rot(y, \Delta t_\beta) Rot(z, \Delta t_\gamma) \\ = \begin{bmatrix} \mathrm{c}(\Delta t_\beta)\mathrm{c}(\Delta t_\gamma) & -\mathrm{c}(\Delta t_\beta)\mathrm{s}(\Delta t_\gamma) & \mathrm{s}(\Delta t_\beta) & \Delta t_x \\ \mathrm{c}(\Delta t_\alpha)\mathrm{s}(\Delta t_\gamma) + C_{21} & \mathrm{c}(\Delta t_\alpha)\mathrm{c}(\Delta t_\gamma) - C_{22} & -\mathrm{s}(\Delta t_\alpha)\mathrm{c}(\Delta t_\beta) & \Delta t_y \\ \mathrm{s}(\Delta t_\alpha)\mathrm{s}(\Delta t_\gamma) - C_{31} & \mathrm{s}(\Delta t_\alpha)\mathrm{c}(\Delta t_\gamma) + C_{32} & \mathrm{c}(\Delta t_\alpha)\mathrm{c}(\Delta t_\beta) & \Delta t_z \\ 0 & 0 & 0 & 1 \end{bmatrix} \\ C_{21} = \mathrm{s}(\Delta t_\alpha)\mathrm{s}(\Delta t_\beta)\mathrm{c}(\Delta t_\gamma), \quad C_{22} = \mathrm{s}(\Delta t_\alpha)\mathrm{s}(\Delta t_\beta)\mathrm{s}(\Delta t_\gamma) \\ C_{31} = \mathrm{c}(\Delta t_\alpha)\mathrm{s}(\Delta t_\beta)\mathrm{c}(\Delta\gamma_s), \quad C_{32} = \mathrm{c}(\Delta t_\alpha)\mathrm{s}(\Delta t_\beta)\mathrm{s}(\Delta t_\gamma) \end{cases} \tag{4}$$

where $Rot(\cdot)$ is the rotation transformation matrix, and $\mathrm{c} = \cos$, $\mathrm{s} = \sin$. The error components contain the position errors $\Delta t_x, \Delta t_y, \Delta t_z$ and the angle errors $\Delta t_\alpha, \Delta t_\beta, \Delta t_\gamma$, which are along or around the reference axis XYZ. The obtaining methods will be given in the following section.

In order to describe the processing errors of the workpiece between the real and the ideal forming process quantitatively, the position and orientation error model mapping from $\{W\}$ to $\{T\}$ are derived step by step through the flame-cutting state and the transformation matrix given in Eqs. (1) to (4).

First, the implicit equations for the nominal parameters of the active joint variables of the machine tool are constructed by using the ideal cutting point $\boldsymbol{p}^{W}$ $(P_x^{w} \quad P_y^{w} \quad P_z^{w})$ on the workpiece, the ideal transformation matrix models, and the flame-cutting process constraints [1]. These can also be obtained as shown in Eqs. (5) to (7).

$$\begin{bmatrix} \boldsymbol{p}^{T} \\ 1 \end{bmatrix} = \left({}^{R}\mathbf{T}_{T}^{ideal} \right)^{-1} \cdot {}^{R}\mathbf{T}_{W}^{ideal} \cdot \begin{bmatrix} \boldsymbol{p}^{W} \\ 1 \end{bmatrix} = \left({}^{R}\mathbf{T}_{S}^{ideal} \cdot {}^{S}\mathbf{T}_{T}^{ideal} \right)^{-1} \cdot \begin{bmatrix} \boldsymbol{p}^{W} \\ 1 \end{bmatrix} \tag{5}$$

$$\begin{cases} f^T\left(\boldsymbol{T}_0,\, \boldsymbol{p}^T\right) = d_{bevel}, \quad \Phi^T\left(\phi_{bevel},\, \left\langle \boldsymbol{T}_0\boldsymbol{p}^T, \boldsymbol{OZ}^T \right\rangle\right) = 0 \\ \begin{bmatrix} \boldsymbol{OZ}^T \\ 1 \end{bmatrix} = \left({}^R\mathbf{T}_T^{ideal}\right)^{-1} \cdot \begin{bmatrix} \boldsymbol{OZ}^R \\ 1 \end{bmatrix}, \quad \begin{matrix} \boldsymbol{T}_0 = \begin{bmatrix} 0 & 0 & 0 \end{bmatrix}^{\mathrm{T}} \\ \boldsymbol{OZ}^R = \begin{bmatrix} 0 & 0 & 1 \end{bmatrix}^{\mathrm{T}} \end{matrix} \end{cases} \tag{6}$$

$$\Theta = \begin{bmatrix} \theta_1 & \theta_2 & \theta_3 & \theta_4 & \theta_5 \end{bmatrix} = Inverse({}^S\mathbf{T}_T^{ideal}) \tag{7}$$

where $\boldsymbol{p}^W, \boldsymbol{p}^T$ are the nominal coordinates of the ideal cutting point described in $\{W\}$ and the position coordinates described in $\{T\}$, $\langle\cdot\rangle$ is the vector operator in the inner product operation, f^T is the position constraint function and is determined by the offset distance d_{bevel} of the flame-cutting procedures, Φ^T is the angle constraint function and is determined by the ideal cutting angle ϕ_{bevel} of the workpiece. $Inverse(\cdot)$ is the solved equation set of the active joint variables. The symbolic expressions can be obtained by using the nominal parameters of the kinematic chain of the machine tool.

Then, substituting the nominal joint variables Θ into Eq. (2), the continuous product expression can be obtained as given by Eq. (8):

$${}^W\mathbf{T}_T^{real} = \left({}^R\mathbf{T}_W^{real}\right)^{-1} \cdot {}^R\mathbf{T}_S^{real} \cdot {}^S\mathbf{T}_T^{real} = {}^R\mathbf{T}_S^{real} \cdot {}^S\mathbf{T}_T^{real} \tag{8}$$

Finally, through the offset vector of the mapping point of the cutting tool, the position processing error models in $\{W\}$ are derived and expressed as:

$$\begin{cases} \begin{bmatrix} Q_x^{\,w} & Q_y^{\,w} & Q_z^{\,w} & 1 \end{bmatrix}^{\mathrm{T}} = {}^W\mathbf{T}_T^{real} \cdot \begin{bmatrix} 0 & 0 & d_{bevel} & 1 \end{bmatrix}^{\mathrm{T}} \\ \Delta x = Q_x^{\,w} - \left(P_x^{\,w} + \Delta p_{x,w}\right), \quad \Delta y = Q_y^{\,w} - \left(P_y^{\,w} + \Delta p_{y,w}\right) \\ \Delta z = Q_z^{\,w} - \left(P_z^{\,w} + \Delta p_{z,w}\right) \end{cases} \tag{9}$$

where $Q_x^{\,w}, Q_y^{\,w}, Q_z^{\,w}$ are the mapping coordinates of the origin within $\{T\}$ on the workpiece, and $\Delta p_{x,w}, \Delta p_{y,w}, \Delta p_{z,w}$ are the integrated errors of the ideal cutting points on the contour boundary of the workpiece.

Meanwhile, according to the ideal vector $\boldsymbol{P}_1\boldsymbol{P}_2$ and the actual vector $\boldsymbol{Q}_1\boldsymbol{Q}_2$ of the cutting contour boundary, the orientation processing error models are derived and expressed as:

$$\begin{cases} \boldsymbol{A}=\begin{bmatrix} P_{x1}-P_{x2} & P_{y1}-P_{y2} & P_{z1}-P_{z2} \end{bmatrix}^{\mathrm{T}} \\ \boldsymbol{B}=\begin{bmatrix} Q_{x1}-Q_{x2} & Q_{y1}-Q_{y2} & Q_{z1}-Q_{z2} \end{bmatrix}^{\mathrm{T}} \\ \Delta\eta=\arccos\left(\dfrac{\boldsymbol{B}_y}{\|\boldsymbol{B}\|}-\dfrac{\boldsymbol{A}_y}{\|\boldsymbol{A}\|}\right), \quad \Delta\omega=\arccos\left(\dfrac{\boldsymbol{B}_z}{\|\boldsymbol{B}\|}-\dfrac{\boldsymbol{A}_z}{\|\boldsymbol{A}\|}\right) \end{cases} \quad \Delta\varepsilon=\arccos\left(\frac{\boldsymbol{B}_x}{\|\boldsymbol{B}\|}-\frac{\boldsymbol{A}_x}{\|\boldsymbol{A}\|}\right) \tag{10}$$

If the wind line (axis) of the cutting tool is regarded as the kerf of the workpiece, the orientation errors from $\{W\}$ to $\{T\}$ can also be obtained directly and described as:

$$\begin{cases} \Delta\mathbf{R}={}^{W}\mathbf{R}_{T}^{\,real}\cdot\left({}^{W}\mathbf{R}_{T}^{\,ideal}\right)^{-1}, \quad \Delta\varepsilon=\arctan(-\Delta\mathbf{R}_{23}/\Delta\mathbf{R}_{33}) \\ \Delta\eta=\arcsin(\Delta\mathbf{R}_{13}), \quad \Delta\omega=\arctan(-\Delta\mathbf{R}_{12}/\Delta\mathbf{R}_{11}) \end{cases} \tag{11}$$

where $\mathbf{R}$ is the 3×3 order rotation matrix extracted from transformation matrix $\mathbf{T}$, the subscripts denote the row-column location of the element in the appointed matrix.

The processing error models in Eqs. (9) to (11) are entirely derived from the actual mapping relation of the cutting contour on the workpiece, whereby the position $\Delta x,\Delta y,\Delta z$ and the orientation $\Delta\varepsilon,\Delta\eta,\Delta\omega$ error components can describe the inaccurate parameters in the forming process of the cutting system. Moreover, based on the origin and the OZ axis direction vector within $\{T\}$ on the workpiece frame $\{W\}$ [10], the simplified models are given by Eq. (12):

$$\begin{cases} \begin{bmatrix} \mathrm{d}x & \mathrm{d}y & \mathrm{d}z & 0 \end{bmatrix}^{\mathrm{T}}={}^{W}\mathbf{T}_{T}^{\,real}\begin{bmatrix} 0 & 0 & 0 & 1 \end{bmatrix}^{\mathrm{T}}-{}^{W}\mathbf{T}_{T}^{\,ideal}\begin{bmatrix} 0 & 0 & 0 & 1 \end{bmatrix}^{\mathrm{T}} \\ \begin{bmatrix} \mathrm{d}\varepsilon & \mathrm{d}\eta & \mathrm{d}w & 0 \end{bmatrix}^{\mathrm{T}}=\arccos\left({}^{W}\mathbf{T}_{T}^{\,real}\begin{bmatrix} 0 & 0 & 1 & 0 \end{bmatrix}^{\mathrm{T}}\right)- \\ \qquad\qquad\qquad\qquad \arccos\left({}^{W}\mathbf{T}_{T}^{\,ideal}\begin{bmatrix} 0 & 0 & 1 & 0 \end{bmatrix}^{\mathrm{T}}\right) \end{cases} \tag{12}$$

Thus, combining the cutting constraint conditions with error models of the CNC flame processing system, the compensation models can be obtained for further derivation, where the implicit calculation expressions of the active joint compensation parameters of the machine tool are expressed as:

$$\begin{aligned} &{}^{W}\mathbf{T}_{T}^{comp}={}^{R}\mathbf{T}_{S}^{\,real}\cdot{}^{S}\mathbf{T}_{T}^{\,comp} \\ &{}^{S}\mathbf{T}_{T}^{comp}=\Delta\mathbf{T}^{thermal}\cdot{}^{S}\mathbf{T}_{T}^{c}(\Theta^{a})=\Delta\mathbf{T}_{T}^{thermal}\cdot\left[{}^{S}\mathbf{T}_{T}^{\,e}(\Theta+\Delta\Theta)\right] \end{aligned} \tag{13}$$

$$\begin{cases} a_x^w=P_x^w+\Delta x, \quad a_y^w=P_y^w+\Delta y, \quad a_z^w=P_z^w+\Delta z \\ \begin{bmatrix} a_x^w & a_y^w & a_z^w & 1 \end{bmatrix}^{\mathrm{T}}={}^{W}\mathbf{T}_{T}^{comp}\cdot\begin{bmatrix} 0 & 0 & d_{bevel} & 1 \end{bmatrix}^{\mathrm{T}} \end{cases} \tag{14}$$

$$\begin{cases} {}^{W}\mathbf{T}_{T}^{comp}\cdot\begin{bmatrix}0\\0\\1\\0\end{bmatrix}={}^{W}\mathbf{T}_{T}^{ideal}\cdot\begin{bmatrix}0\\0\\1\\0\end{bmatrix}+\begin{bmatrix}\Delta\varepsilon\\\Delta\eta\\\Delta w\\0\end{bmatrix}, \begin{bmatrix}O_x^w\\O_y^w\\O_z^w\\1\end{bmatrix}={}^{W}\mathbf{T}_{T}^{comp}\cdot\begin{bmatrix}0\\0\\0\\1\end{bmatrix} \\ \phi_{bevel}=\operatorname{acos}\left[\left|O_z^w-a_z^w\right|\Big/\sqrt{\left(O_x^w-a_x^w\right)^2+\left(O_y^w-a_y^w\right)^2+\left(O_z^w-a_z^w\right)^2}\right] \end{cases} \tag{15}$$

where a_x^w, a_y^w, a_z^w are the prediction parameters of the actual cutting points in $\{W\}$, ${}^{W}\mathbf{T}_{T}^{comp}$ is the compensation matrix between $\{W\}$ and $\{T\}$, and $\Delta\Theta$ are the compensation values of the active joint variables.

In accordance with Eqs. (13) to (15), processing error compensation motion can be realized for the CNC flame-cutting machine. During operation, both the prediction and the compensation parameters for the processing errors can be obtained after substituting the geometric errors obtained from off-line calibration and the thermal deformations obtained from on-line calculation into the established models. Especially when the thermal deformations are transient temperature variations, the abovementioned models and the actual cutting process should also have real-time and accurate integrity performance. It is worth pointing out that in the process of improving the accuracy of the processing system, the test items and procedures in the ISO 230 standards are referred but not completely adopted in this investigation. Although the established theoretical models are different from the test experiments of those standards, they still have some connection to the present research purpose. For instance, in addition to the processed workpiece and the actual cutting conditions, both the geometric errors and the thermal deformations included in the machine tool are considered, which can be identified and corrected respectively. The geometric error modifications are all carried out only when the driving errors of the active joints have been corrected in advance, and a similar analysis frame is adopted to construct the on-line calculation models of the thermal deformations.

3 FEA Testing Procedures for Thermal Deformation Elements

Because of the inadequacy of in-situ sensing technology for thermal deformation measurement in the high-temperature state of the flame-cutting process, this section presents the FEA testing procedures [15] to obtain off-line data of thermal deformation and temperature-field variation under varied working conditions. Taking the 1/12 circumferential configuration of a straight-

cutting task as the specified application example, a brief description of the setup steps of the FEA simulation in ANASY is as follows:

1. Importing the entity model and meshing. Importing the CAD model related to the fixed cutting configuration; the model was meshed using Solid-95 elements and an uneven meshing technique. Meshing revealed a total of 5,199,077 elements and 7,858,866 nodes. Figure 3 shows the meshed assembly of the whole processing system, where small details such as fillets and chamfers were neglected.

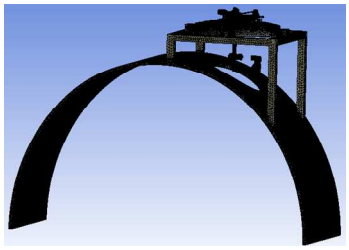

Figure 3 Meshed model of the fixed cutting configuration of the CNC flame processing system.

2. Setting the material properties. According to the structural properties of the processing system, the major materials are low-carbon steel, brass etc. And the temperature variation laws of the thermal-mechanical parameters are set based on the practical iron and steel material standards [16].
3. Appling temperature and displacement boundary conditions. The model in Figure 3 under research has three major temperature constraints [15]: (a) contact resistance within the 151 combined surfaces is set to $2520\mathrm{W/(m^2 \cdot {}^\circ C)}$; (b) composite heat transfer (convection and radiation) coefficient is applied to the end of the processing system, where the tool surface is set to $60\mathrm{W/(m^2 \cdot {}^\circ C)}$, the workpiece surface is set to $45\mathrm{W/(m^2 \cdot {}^\circ C)}$, and the rest surface is set to $25\mathrm{W/(m^2 \cdot {}^\circ C)}$; (c) natural convection is applied to the frame and front components, and the overall surfaces are set to $10\mathrm{W/(m^2 \cdot {}^\circ C)}$. The displacement boundary condition is that the interfaces of the workpiece are in completed constraint state.
4. Applying temperature loads. According to the operating conditions of the specific configuration and the theoretical models of the heat source power [17], the input temperature loads for the heat sources can be obtained. The major changing laws are shown in Figure 4, while the input temperature of the 9 moving parts are given by the harmonic form $T = 24 + 2(1 - \cos(\pi t/20))\ ^\circ\mathrm{C}$ and omitted in the curve form.

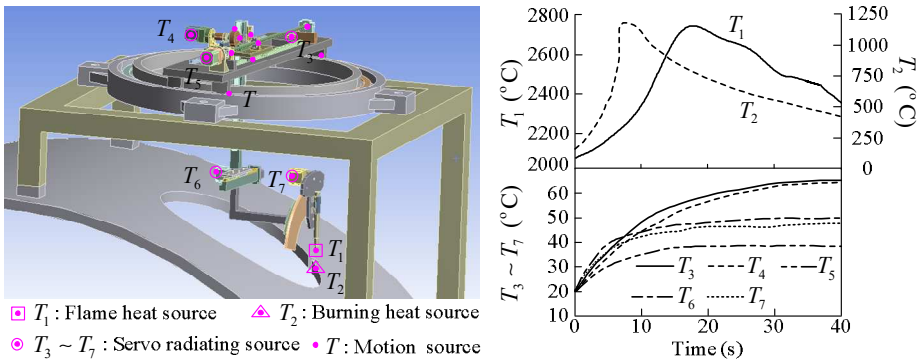

Figure 4 Locations and changing laws of the heat sources in the FEA model.

5. Adopting the initial conditions for the thermal structure simulation. The initial condition for the temperature calculation is given as the referred temperature, which is set to 20°C. The input loads for the deformation calculation are the obtained temperature data, and the initial conditions only require a gravity environment. Referring to the flame-cutting procedure, the simulation time is set to 40 s and the calculation step is 1 s.

Based on the FEA simulation conditions mentioned above, the numerical results for the fixed cutting configuration can be obtained. They are shown in Figure 5. Among them, the temperature field and the deformation field at the later 30 s are given in Case (a), which shows the transient temperature state and the thermal deformation state of the flame processing system. Case (b) shows the thermal deformation series results, where the input is the temperature rising of T_1 and the output is the deformation in the Z direction of $\{W\}$, which is the supporting point at the right end of the frame of the machine tool.

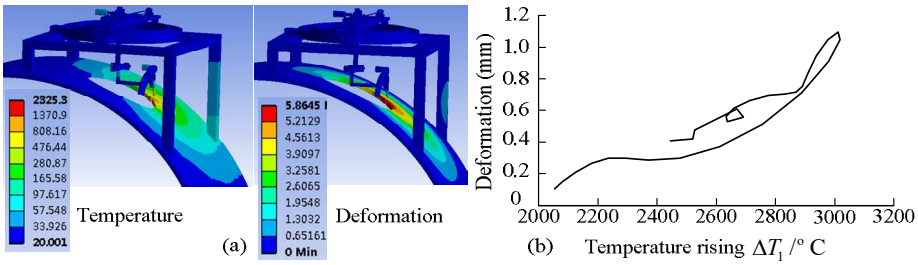

Figure 5 Overall results for the fixed-cutting configuration: (a) temperature and deformation field at the final 30 s, (b) thermal deformation responses.

From the overall results shown in Figure 5, it is known that the thermal deformation changes positively corresponds to the positive growth trend in the

rising phase. When the temperature decreases, the related deformation also decreases, but a few deviations appear while comparing with the values of the increase stage. The obtained results show that the thermal deformation caused by the changeable heat sources has pseudo-hysteresis effects [18], which create different thermal influences when the system temperature rises and falls down to the same parameters.

Note that, to make the FEA model consistent with the actual cutting situation, in this section a specified point calculation is conducted in the fixed-cutting configuration instead of adopting a moving heat source and life-death element technology to simulate the completed process. Therefore, the obtained results are only applicable to the current position and its nearby areas, which is the minimum unit in the testing environment. After adjusting the specific configuration through the flame-cutting process, all the thermal deformation test results could be obtained by a similar simulation process. Moreover, although the assembly structure that included geometric errors is not used in this section, a simplified ideal model could ensure the feasibility of the calculation and improve the efficiency of the FEA model, which may bring on a few facultative and inconsistent detection errors in theory.

4 Thermal Dynamics Models of Thermal Deformation

The thermal deformations are connected to several structural units of the processing system, which means that a single thermal error output relates to multiple temperature inputs. Therefore, after obtaining the discrete time-series between the temperatures and the thermal errors from the original temperature and deformation field, the multiple-input single-output models are applied to establish the thermal dynamics models.

Taking the end point's deformation $\Delta t_x^{\mathrm{T}} \to \Delta \mathbf{T}_T^{thermal}$ in the X direction as an example, the time sequences of the temperature and deformation elements are first extracted from the calculation results based on the fixed-cutting configuration, and the distribution of the temperature measuring points is also preset based on the strategy of main factors [19], as shown in Figure 6.

Besides, Case (a) shows the spatial distribution of the 9 initial measuring points, of which contains 4 major heat sources $\#01,\#02,\#03,\#04$ and 5 non-heating positions $\#1,\#2,\#3,\#4,\#5$, which are chosen by the temperature gradient field and the feasible imaging area of the infrared camera device [20] in the fixed-assembly condition. Case (b) shows the original testing data of the temperature and deformation elements, which mainly includes the changing laws of $\#1,\#2,\#3,\#4,\#5$ and the thermal error results of the target point.

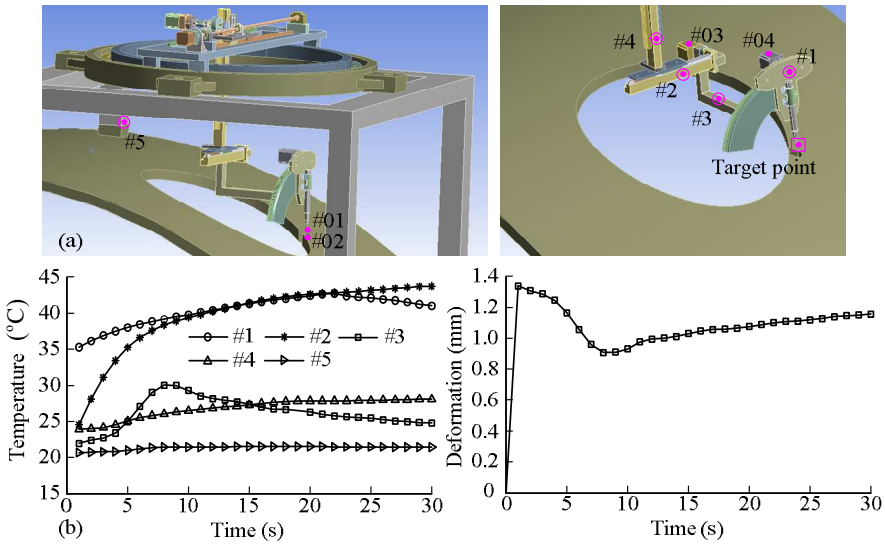

Figure 6 Extracted calculation results based on the fixed-cutting configuration: (a) spatial distribution of the 9 initial measuring points, (b) time sequences of temperature and the target point deformations in the X direction.

Table 2 Synthetic Grey Correlation of Data Serials of Measuring Points

No.	#01	#02	#03	#04	#1	#2	#3	#4	#5
#01	1.000	0.739	0.539	0.537	0.511	0.531	0.509	0.506	0.501
#02		1.000	0.519	0.518	0.505	0.515	0.504	0.503	0.501
#03			1.000	**0.969**	0.635	0.898	0.615	0.576	0.518
#04				1.000	0.644	**0.924**	0.622	0.581	0.520
#1					1.000	0.670	**0.925**	0.782	0.568
#2						1.000	0.644	0.596	0.523
#3							1.000	0.832	0.580
#4								1.000	0.620
#5									1.000
Deformation	**0.505**	**0.502**	0.505	0.514	**0.513**	**0.506**	0.512	**0.514**	**0.523**

Before constructing the thermal dynamics models, the key temperature measuring points are selected using the optimization process. As shown in Table 2, the coefficient matrix of the synthetic grey correlation [21] is obtained between the temperature data serial of thermal points and thermal error data serial. Then, by setting the threshold value to 0.9, the placed thermal points can be grouped and merged to {#01}, {#02},{#01}, {#02}, {#03/#04/#2}, {#1/#3}, {#4}, {#5}. Finally, the critical points are picked out according to the synthetic grey correlation results for different groups and are described as {#01},{#02},{#1},{#2},{#4},{#5}.

Furthermore, the six candidate points can produce 63 combinations. By calculating the synthetic grey correlation between the result serial of each model and the actual thermal error data serial, models of every possible compounding of the picked out points are evaluated to decide the critical thermal points. As shown in Figure 7, the final key thermal points can be optimized and selected as $\{\#01\},\{\#02\},\{\#2\},\{\#5\}$ by comparing the correlation of different combinations and the tracking results, respectively. Apart from that, the explicit expression of the thermal dynamic model [22] with four inputs and one single output is given by:

$$\begin{cases} \mathrm{d}T_i(t) = T_i(t) - T_i(t-1), \quad \mathrm{d}E_x(t) = E_x(t) - E_x(t-1), \quad i = 1,2,3,4 \\ \mathrm{d}E_x(t) = 0.1573 \cdot \mathrm{d}E_x(t-1) + 0.1746 \cdot \mathrm{d}E_x(t-2) + \\ \qquad 0.0258 \cdot \mathrm{d}T_1(t) - 0.0504 \cdot \mathrm{d}T_2(t) - 0.1679 \cdot \mathrm{d}T_3(t) - \\ \qquad 2.3146 \cdot \mathrm{d}T_4(t) - 0.0196 \cdot \mathrm{d}T_1(t-1) + 0.0363 \cdot \mathrm{d}T_2(t-1) - \\ \qquad 0.1142 \cdot \mathrm{d}T_3(t-1) - 3.4205 \cdot \mathrm{d}T_4(t-1) - 0.0117 \cdot \mathrm{d}T_1(t-2) - \\ \qquad 0.0142 \cdot \mathrm{d}T_2(t-2) - 0.1329 \cdot \mathrm{d}T_3(t-2) + 1.6301 \cdot \mathrm{d}T_4(t-2) \\ E_x(t) = \mathrm{d}E_x(1) + \mathrm{d}E_x(2) + \cdots + \mathrm{d}E_x(t-1) + \mathrm{d}E_x(t) \end{cases} \tag{16}$$

where $T_1(t),T_2(t),T_3(t),T_4(t)$ are the data sequences of the key thermal points $\{\#01\},\{\#02\},\{\#2\},\{\#5\}$, $E_x(t)$ is the time sequence of the thermal deformation in the X direction for the end point, $\mathrm{d}T_i(t)$ and $\mathrm{d}E_x(t)$ are the input/output time series after the first-differenced transformation.

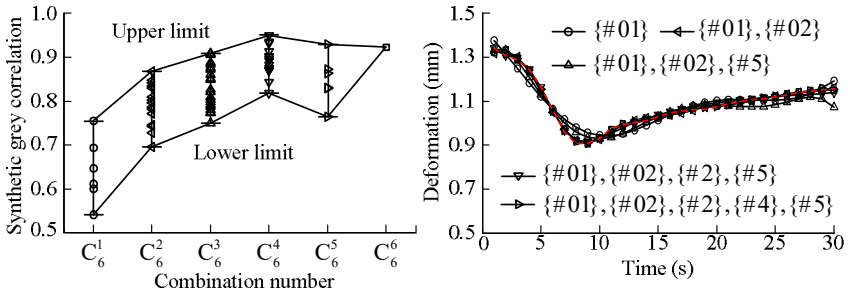

Figure 7 Optimization of thermal points for the X direction deformation of the end point.

Figure 8 shows the validated results of the established model given in Eq. (16). Apart from that, Case (a) shows the modeled outputs and the residual errors with respect to the optimal thermal points. The tracking results where the error interval is within ±0.05 mm indicate that the best accuracy and tracking performance for the thermal dynamic models can be obtained by using the key thermal points. Case (b) shows the prediction effects of the established model,

while the inputs are the temperature data from 31 s to 40 s in the FEA simulation and the validation values are extracted from the calculation results. It can be seen that although the errors in this stage are larger than the tracking errors in the modeling process, the variation range is only within ± 0.1 mm, which means the model can predict the thermal errors based on the current configuration accurately.

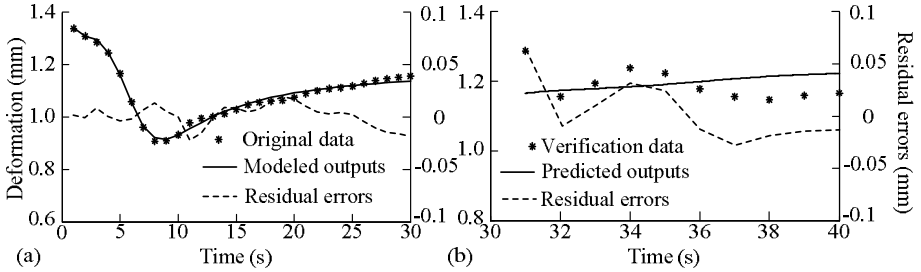

Figure 8 Validation results of the thermal dynamics model: (a) tracking performance, (b) prediction effects.

Table 3 Components of thermal errors and integrated error matrix $\Delta\mathbf{T}^{thermal}$.

Terms	Fixed cutting configuration	Groups	Error elements
$\Delta\mathbf{T}_S^{thermal}$	Four supporting points of the machine's frame	$4\times\{E(t)\}$	Implicit function for 6 components f_S
$\Delta\mathbf{T}_T^{thermal}$	Two end points of the cutting tool's axis	$2\times\{E(t)\}$	Applied 3 position components directly Implicit function for 3 orientation components f_T

It should be mentioned that only the temperature variables are contained in the established dynamic model, while the position elements are not taken into account since the applied temperature and deformation data are only related to fixed-cutting configuration $C(i)$, $i\in\{1,\cdots,M\}$. For the M configurations involved in the whole process cycle, the above modeling procedures should be repeated M times to meet the on-line prediction requirements. By referring to the topological structures of the CNC flame processing system, the required components of transformation matrix $\Delta\mathbf{T}^{thermal}$ are shown in Table 3, because some of those elements cannot be substituted directly. However, when the explicit models of the overall elements are similar to the expression given in Eq. (16) and the implicit functions f_S, f_T can also be easily determined by a simple space geometry relationship [22], those iterant contents are omitted in this section.

5 Results of Experimental Studies

For the CNC flame-cutting machine and spatial surface operating conditions shown in Figure 1, experimental studies were conducted to verify the validity of the accuracy enhancement method. The geometric errors were obtained by the kinematics calibration and the thermal dynamics models of the thermal deformations were carried out in advance. Figure 9 shows the actual cutting environment of the comparison experiments between the proposed method and the teaching method, both referring to Figure 1. It should be noted that the teaching method for programming instead of off-line programming was taken to be the compared type in the experimental studies. The reasons were that it not only is currently the main way to improve the accuracy of the flame-cutting process and is practical for spatial surface situations, it also has similar properties as the proposed method, which could make the processed workpiece obtain a higher cutting accuracy than the machine tool.

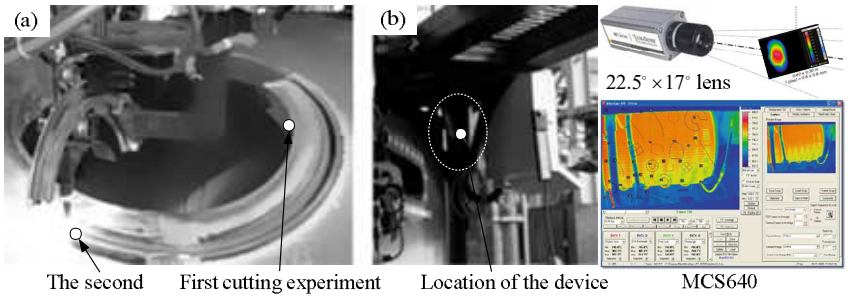

Figure 9 Actual cutting environment: (a) comparison experiments between the teaching method and the proposed method, (b) detection device MCS640.

The first cutting experiment in Case (a) was implemented through the teaching method, which achieves the forming process of a groove profile by using geometric inspection data for the workpiece and constructing a feedback correction table. The second cutting experiment was implemented through the proposed method, which was done with prediction data of the processing errors and compensation values for every cutting configuration. Case (b) shows the on-line temperature detection device MCS640 used in the experiments. It is fixed on the top corner of the frame and has a maximum distance of around 2.0 m from the key thermal points on the end-effector. After temperature calibration, the device can be used to obtain the cutting thermal imager with a $22.5^{\circ} \times 17^{\circ}$ lens, while the true surface temperatures of objects are extracted by matching software [20].

Figure 10 shows images of the cutting effect after the comparison experiments, which contain both a local amplification and a micro-show of the surface of a

straight contour. By analyzing the roughness and visible quality of the groove surface, it was found that the results in the second set were better than the first set as a whole. The results 'initially and directly' indicate that the proposed method can effectively improve the cutting quality of a workpiece compared to the teaching method. The established models are correct and rational.

Figure 10 Local amplification and micro-show of the cutting effect of a straight contour.

Table 4 Testing results of straight groove profiles of forming workpiece

Terms		Teaching method	Proposed method
Accuracy	Dimensional tolerances (mm)	[-0.7, 1.8]	[-0.5, 1.1]
	Perpendicularity tolerances (mm)	1.2	0.7
Quality	Roughness	25	12.5
	Straightness (mm)	0.8	0.5

As for the straight contours from the comparison experiments, after cleaning up the defects that hinder measurement and division of the quality grade in the cutting surface, the straight groove profiles were tested based on DIN2310 [23]. Taking the upper edge of the profile as reference mark and selecting 36 measuring points around the whole circle, the testing results of the forming workpiece were obtained, as shown in Table 4 and Figure 11. The dimensional tolerances described by the interval parameters are the limit deviations (algebraic difference) between the ideal dimensions and the actual testing dimensions of the forming profile, while the actual detection values were achieved by using a steel ruler. One estimated reading is uncertainty in millimeters. The perpendicularity tolerances are equivalent to the maximum distances between two parallel straight lines that limit the cut face profile at 90°, while the lines are situated in a plane, normal to both the workpiece surface and the cut face. The actual detection values were achieved by using an extra fine grade rectangular ruler. The mean height of the profile (roughness) was determined by quality samples and a craftsman from the workshop. The straightness was determined with a steel wire with a diameter of less than 0.5 mm. These readings are both related to the error limit of the measuring instrument. Moreover, the dimension errors of the measuring points were also mapped to the XOY plane and represented in a polar coordinate system. The

angular error around the Z axis was obtained and derived from the perpendicularity tolerance results.

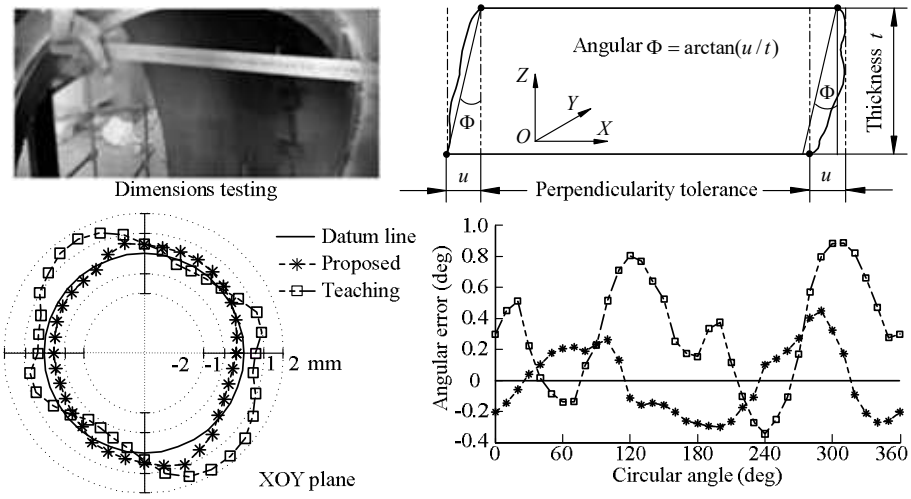

Figure 11 Quantitative testing results of the straight groove profiles.

From the quantitative testing results shown in Figure 9 and Table 3, it can be seen that the accuracy enhancement of the proposed method is impressive. Compared to the teaching method, the maximum dimensional error was reduced from 1.8 mm to 1.1 mm, the mean value was reduced from 1.14 mm to 0.68 mm, the perpendicularity tolerances were reduced from 1.2 mm to 0.7 mm, the maximum angular error of the profile edge was reduced from 0.8893° to 0.5207°, and the mean parameter was reduced from 0.3974° to 0.2062°. Furthermore, it was also shown that the dimensional tolerances increased with 38.9%, the perpendicularity tolerances increased with 41.7%, and the straightness decreased with 37.5%.

The quantitative comparison results 'deeply' verified the effectiveness of the proposed method and also showed that a higher performance can be achieved with the CNC flame-cutting machine. The main reasons are that the proposed method not only takes into account the geometric errors involved in both the workpiece and the machine tool, but also considers the real-time thermal errors caused by the non-uniform temperature field during the flame-cutting process. It can accurately predict the processing errors of the workpiece and make modifications by adopting the compensation way on-line based on every cutting configuration of the machine tool, which improves the cutting accuracy effectively in the actual processing phase and ensures the cutting quality of the final forming profiles.

6 Conclusions

In this paper, an accuracy enhancement method was proposed for a CNC flame-cutting machine used in spatial surface operating conditions, which can improve cutting quality by modeling prediction and compensating processing errors during the real-time cutting process. Specifically, based on the homogeneous transformation matrix of the machining coordinate systems, processing error prediction models were established to derive the position and orientation errors of the workpiece, of which the geometric error terms were determined by calibration in advance, while the thermal deformation elements are obtained on-line. Combined with the flame-cutting parameters, real-time compensation models were constructed to ensure the accuracy of the forming process of the machine tool.

In addition, the validity of the accuracy enhancement method was verified through comparison with the general teaching method in a number of experiments. The results of the comparison experiments showed that when the proposed method was applied to the actual cutting process, the dimensional accuracy increased 38.9%, the perpendicularity tolerances increased 41.7%, and the straightness decreased 37.5% relative to the teaching method. The overall results indicate that the proposed method is effective and rational in considering the thermal effects in on-line form. Through adjusting the obtained prediction and compensation models, the proposed method can also be used under any working conditions in the future.

Acknowledgments

This work is a cross-sequential research of a project that is supported by the National Natural Science Foundation of China (Grant No. 51175099). The authors would like to thank China Bohai Shipbuilding Heavy Industry Co Ltd for their assistance with the experiments.

References

[1] Li, Y.J., *Cutting Technology and Application*, Beijing: Chemical Industry Press, 2004.

[2] Ramesh, R., Mannan, M.A. & Poo, A.N., *Error Compensation in Machine Tools – a Review Part I: Geometric, Cutting-Force induced and Fixture-Dependent Errors*, International Journal of Machine Tools and Manufacture, **40**(9), pp. 1235-1256, 2000.

[3] Ramesh, R., Mannan, M.A. & Poo, A.N., *Error Compensation in Machine Tools – a Review Part II: Thermal Errors*, International Journal of Machine Tools and Manufacture, **40**(9), pp. 1257-1284, Jul. 2000.

[4] Zhu, W.D., Wang, Z.G. & Yamazaki, K., *Machine Tool Component Error Extraction and Error Compensation by Incorporating Statistical Analysis*, International Journal of Machine Tools and Manufacture, **50**(9), pp. 798-806, 2010.

[5] Chen, G., Li, T., Chu, M., Jia, Q.X. & Sun, H.X., *Review on Kinematics Calibration Technology of Serial Robots*, International Journal of Precision Engineering and Manufacturing, **15**(8), pp. 1759-1774, 2014.

[6] Yuan, Z.H. & Huang, J., *Research on Cutting Error Compensation of Numerical Control Pipe-Cutting Machine*, Journal of Wuhan University of Technology, **23**(4), pp. 64-67, 2001.

[7] Song, W.K., Wang, G., Xiao, J.L., Wang, G.D. & Hong, Y., *Research on Multi-Robot Open Architecture of an Intelligent CNC System based on Parameter-Driven Technology*, Robotics and Computer-Integrated Manufacturing, **28**(3), pp. 326-333, 2012.

[8] Decker, K., *Modern Cutting Machines and Techniques in Shipbuilding Industry*, Svetsaren (English Edition), **57**(1), pp. 22-26, Sep. 2002.

[9] Mayr, J., Jedrzejewski, J. & Uhlmann, E., *Thermal Issues in Machine Tools*, CIRP Annals-Manufacturing Technology, **61**(2), pp. 771-791, 2012.

[10] Srivastava, A.K., Veldhuis, S.C. & Elbestawit, M.A., *Modeling Geometric and Thermal Errors in a Five-Axis CNC Machine Tool*, International Journal of Machine Tools and Manufacture, **35**(9), pp. 1321-1337, Sep. 1995.

[11] Li, Z.H., Yang, J.G., Fan, K.G. & Zhang, Y., *Integrated Geometric and thermal Error Modeling and Compensation for Vertical Machining Centers*, The International Journal of Advanced Manufacturing Technology, **76**(5), pp. 1139-1150, 2015.

[12] Hu, S.H., Zhang, M.H., Zhang, B.P., Chen, X. & Yu, W., *Design and Accuracy Analysis of a Metamorphic CNC Flame Cutting Machine for Ship Manufacturing*, Chinese Journal of Mechanical Engineering, **29**(5), pp. 930-943, 2016.

[13] Schroer, K., Albright, S., Grethlein, M. & Grethlein, M., *Complete, Minimal and Model-Continuous Kinematic Models for Robot Calibration*, Robotics and Computer-Integrated Manufacturing, **13**(1), pp. 73-85, Mar. 1997.

[14] He, R.B., Zhao, Y.J., Yang, S.N. & Yang, S.Z., *Kinematic-Parameter Identification for Serial-Robot Calibration based on POE Formula*, IEEE Transactions on Robotics, **26**(3), pp. 411-423, Jun. 2010.

[15] Mian, N.S., Fletcher, S., Longstaff, A.P. & Myers, A., *Efficient Thermal Error Prediction in a Machine Tool Using Finite Element Analysis*, Measurement Science and Technology, **22**(8), pp. 1-10, 2011.

[16] Yu, L.L. & Zeng, Z.M., *Handbook of Practical Iron and Steel Materials*, Beijing: China Machine Press, 2001.

[17] Thiébauda, R., Drezetb, J.M. & Lebeta, J.P., *Experimental and Numerical Characterisation of Heat Flow During Flame Cutting of Thick Steel Plates*, Journal of Materials Processing Technology, **214**(2), pp. 304-310, 2014.

[18] Attia, M.H. & Fraser, S., *A Generalized Modeling Methodology for Optimized Real-Time Compensation of Thermal Deformation of Machine Tools and CMM Structures*, International Journal of Machine Tools and Manufacture, **39**(8), pp. 1001-1016, 1999.

[19] Yang, J.G., Yuan, J.X. & Ni, J., *Thermal Error Mode Analysis and Robust Modeling for Error Compensation on a CNC Turning Center*, International Journal of Machine Tools and Manufacture, **39**(9), pp. 1367-1381, 1999.

[20] Li, Y.H., Sun, X.G. & Yuan, G.B., *Accurate Measuring Temperature with Infrared Thermal Imager*, Optics and Precision Engineering, **15**(9), pp. 1336-1341, 2007.

[21] Li, Y.X., Yang, J.G., Gelvis, T. & Li, Y.Y., *Optimization of Measuring Points for Machine Tool Thermal Error based on Grey System Theory*, The International Journal of Advanced Manufacturing Technology, **35**(7), pp. 745-750, Jan. 2008.

[22] Yang, H. & Ni, J., *Adaptive Model Estimation of Machine Tool Thermal Errors based on Recursive Dynamic Modeling Strategy*, International Journal of Machine Tools and Manufacture, **45**(1), pp. 1-11, 2005.

[23] ISO 9013, D.I.N.E.N. 12, *Thermal Cutting-Classification of Thermal Cuts-Geometrical Product Specification and Quality Tolerances*, 2014.